

RESEARCH

Open Access



# Scalable production of anti-inflammatory exosomes from three-dimensional cultures of canine adipose-derived mesenchymal stem cells: production, stability, bioactivity, and safety assessment

Anatcha Thongsit<sup>1,3,4</sup>, Saranyou Oontawee<sup>2,3,4</sup>, Parkpoom Siriarchavatana<sup>2,3,4</sup>, Watchareewan Rodprasert<sup>3,4</sup>, Poorichaya Somparn<sup>6</sup>, Daneeya Na Nan<sup>7,8</sup>, Thanaphum Osathanon<sup>9,10,11</sup>, Hiroshi Egusa<sup>12</sup> and Chenphop Sawangmake<sup>3,4,5,11\*</sup>

## Abstract

**Background** The therapeutic potential of exosomes derived from mesenchymal stem cells (MSCs) is increasingly recognized in veterinary medicine. This study explored the feasibility of a microcarrier-based three-dimensional (3D) culture system for producing the exosomes (cEXO). Investigations were conducted to enhance production efficiency, ensure stability, and evaluate the therapeutic potential of cEXO for anti-inflammatory applications while assessing their safety profile.

**Results** The microcarrier-based 3D culture system improved efficient production of cEXO, yielding exosomes with acceptable profiles, including a size of approximately 81.22 nm, negative surface charge, and high particle concentration ( $1.32 \times 10^9$  particles/mL). Confocal imaging proved dynamic changes in cell viability across culture phases, highlighting the challenges of maintaining cell viability during repeated exosome collection cycles. Characterization via transmission electron microscopy, nanoparticle tracking analysis, and zeta-potential measurements confirmed the stability and functionality of cEXO, particularly when stored at  $-20^\circ\text{C}$ . Functional assays showed that cEXO exerted significant anti-inflammatory activity in RAW264.7 macrophages in an inverse dose-dependent manner, with no observed cytotoxicity to fibroblasts or macrophages. Acute toxicity testing in rats revealed no adverse effects on clinical parameters, organ health, or body weight, supporting the safety of cEXO for therapeutic use.

**Conclusions** This study highlights the potential of a microcarrier-based 3D culture system for scalable cEXO production with robust anti-inflammatory activity, stability, and safety profiles. These findings advance the development of cEXO-based therapies and support their application in veterinary regenerative medicine.

\*Correspondence:

Chenphop Sawangmake  
chenphop.s@chula.ac.th

Full list of author information is available at the end of the article



© The Author(s) 2025. **Open Access** This article is licensed under a Creative Commons Attribution-NonCommercial-NoDerivatives 4.0 International License, which permits any non-commercial use, sharing, distribution and reproduction in any medium or format, as long as you give appropriate credit to the original author(s) and the source, provide a link to the Creative Commons licence, and indicate if you modified the licensed material. You do not have permission under this licence to share adapted material derived from this article or parts of it. The images or other third party material in this article are included in the article's Creative Commons licence, unless indicated otherwise in a credit line to the material. If material is not included in the article's Creative Commons licence and your intended use is not permitted by statutory regulation or exceeds the permitted use, you will need to obtain permission directly from the copyright holder. To view a copy of this licence, visit <http://creativecommons.org/licenses/by-nc-nd/4.0/>.

**Keywords** Canine adipose-derived mesenchymal stem cells, Exosomes, Microcarrier-based 3D culture, Anti-inflammatory activity, Safety profile

## Background

Exosomes, small extracellular vesicles (30–150 nm in diameter), are increasingly recognized as critical mediators of intercellular communication. They facilitate the transfer of molecular signals, including proteins, lipids, and RNA, between cells and have garnered significant attention for their therapeutic potential, particularly in inflammatory disease management [1]. Mesenchymal stem cells (MSCs), known for their robust immunomodulatory and anti-inflammatory properties, have emerged as a promising source of exosomes for therapeutic applications [2]. Among MSC sources, adipose-derived mesenchymal stem cells (AD-MSCs) stand out due to their abundant availability, ease of isolation, and potent regenerative capacity [3].

The use of three-dimensional (3D) cultures for AD-MSC-derived exosome production holds significant promise for improving both the yield and functionality of these vesicles. While traditional two-dimensional (2D) cultures are limited by their inability to mimic the complex cellular microenvironment *in vivo*, 3D cultures replicate tissue-like architecture more effectively, resulting in exosomes with enhanced biological activity [4]. Exosomes produced from 3D cultures of AD-MSCs have demonstrated superior anti-inflammatory effects, making them particularly beneficial for conditions characterized by excessive inflammation, such as osteoarthritis and inflammatory bowel disease [4–7].

The production of anti-inflammatory exosomes from 3D cultures requires optimized culture conditions to preserve cell viability, proliferative ability, and differentiation potential. Moreover, the isolation process needs stringent purification steps to ensure high yields and avoid contamination, as improper handling may compromise the biological activity of exosomes. Research shows that exosomes derived from AD-MSCs can modulate immune responses by suppressing pro-inflammatory cytokines, promoting the polarization of macrophages into an anti-inflammatory phenotype, and balancing T-cells involved in inflammatory cascades [3, 7, 8].

For clinical translation, the stability, efficacy, and safety of exosomes must be rigorously evaluated. Stability under various storage conditions is crucial for their therapeutic applications, as studies have shown that exosomes maintain their structural integrity and bioactivity over time under low-temperature storage conditions [9]. Despite their natural origin and non-immunogenic properties, exosomes carry potential risks, such as contamination, off-target effects, or long-term immunological responses, which demand thorough investigation. Preclinical

evaluations following ISO 10993-11 guidelines involve acute toxicity testing in rodent models to assess immediate and delayed systemic effects after single or multiple dose administration [10]. Such assessments provide critical data on tolerability, mortality, and organ-specific toxicity. These steps, coupled with clinical trials, are vital to establish a comprehensive safety and efficacy profile, facilitating the transition of exosome-based therapies to clinical applications [11].

This research focuses on producing exosomes from canine adipose-derived mesenchymal stem cells (cAD-MSCs) using a microcarrier-based 3D culture system. Detailed qualitative and quantitative characterization of these exosomes was planned to evaluate their stability under freezing and refrigerating storage conditions. Furthermore, the study aims to assess therapeutic potential through *in vitro* tests, including nitric oxide inhibition in macrophages and fibroblast proliferation assays. Finally, *in vivo* safety was explored via acute toxicity tests involving tail-vein injections in a rat model, with the goal of proving their efficacy and safety for clinical applications.

## Results

### Microcarrier-based 3D culture facilitates scalable production of exosomes from cAD-MSCs

The microcarrier-based 3D culture system shows feasibility for exosome production from cAD-MSCs, as depicted in Fig. 1A. Confocal laser scanning microscopy (CLSM) images (Fig. 1B) reveal the dynamics of live (green) and dead (red) cell populations on polystyrene (PS) microcarriers (blue) across various culture phases. During the seeding phase, intermittent agitation over three hours helped initial cell attachment, with cells showing a rounded morphology. A subsequent 21-hour resting phase allowed firm cell attachment, evident from increased green fluorescence. In the 3-day expansion phase (Day 0), cell proliferation was pronounced, with strong green fluorescence confirming high viability. However, during the serum-free medium (0% FBS medium; VSCBIC-3) incubation on Day 1 for exosome collection, viable cell numbers decreased compared to the expansion phase. The appearance of rounded cells and increased red fluorescence signified heightened cellular stress and death. A 2-day refreshment phase in DMEM-10FBS (Day 3) restored cell viability, with prominent green fluorescence indicating healthy attachment. By Day 4, during a second serum-free medium incubation, cell viability declined further, characterized by an increase in dead cells and a reduction in viable cell numbers. These findings highlight the challenges of sustaining

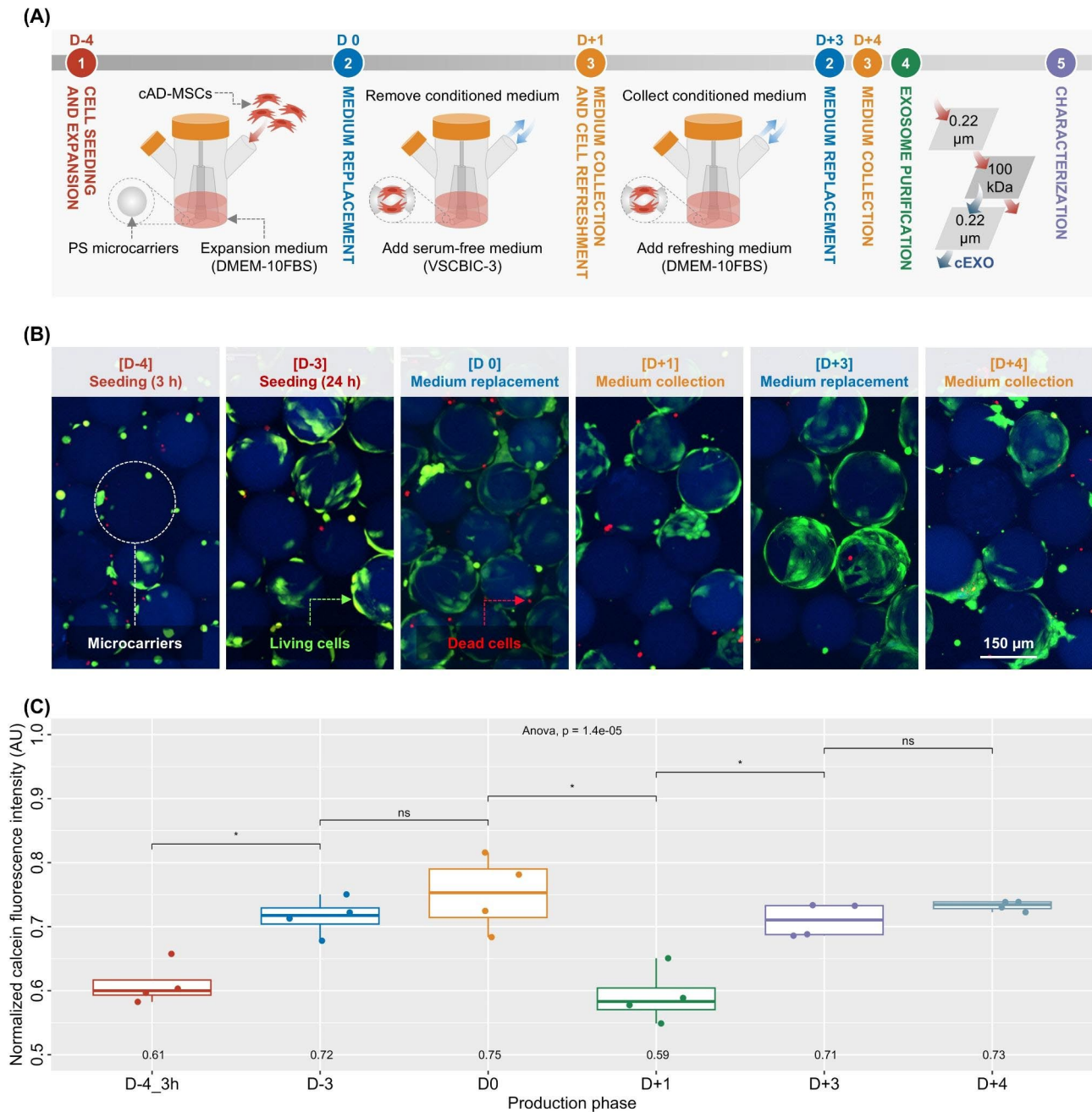


**Fig. 1** Microcarrier-based 3D culture system for exosome production from cAD-MSCs. **(A)** Schematic representation of the culture process, including cell seeding, expansion, medium replacement, and exosome collection. **(B)** CLSM images showing live-dead staining of cAD-MSCs on PS microcarriers (blue) across different production phases. Green indicates live cells, red indicates dead cells, and blue represents PS microcarrier reflection. The scale bar represents 150  $\mu\text{m}$ . **(C)** Boxplot of normalized calcein fluorescence intensity during culture phases, demonstrating significant viability changes. Mean values of each group were annotated at the bottom, and global statistics were stated at the top. The bars indicate pairwise comparisons (ns; no significance or  $p > 0.05$ , \*;  $p \leq 0.05$ ). **Abbreviation:** AU; arbitrary unit, and CLSM; confocal laser scanning microscopy

cell viability during repeated exosome collection cycles, critical for improving 3D culture systems for scalable exosome production.

Quantitative analysis (Fig. 1C) confirms the trends seen in CLSM images, utilizing normalized calcein fluorescence intensities as a proxy for live-cell populations.

During the seeding phase (Day  $-4$ , 3 h), the mean fluorescence intensity was  $0.61 \pm 0.03$  AU, showing initial cell attachment. After the 21-hour resting phase (Day  $-3$ ), the intensity significantly increased to  $0.72 \pm 0.03$  AU ( $p \leq 0.05$ ), reflecting improved cell attachment. During the expansion phase (Day  $-3$  to Day 0), the intensity

further rose to  $0.75 \pm 0.06$  AU, though this increase compared to Day -3 was not statistically significant. On Day 1, following the first serum-free medium incubation, the intensity dropped significantly to  $0.59 \pm 0.04$  AU ( $p \leq 0.05$ ), suggesting reduced cell viability and cellular stress. Upon refreshment with DMEM-10FBS, cell viability improved by Day 3, with a mean value of  $0.71 \pm 0.03$  AU ( $p \leq 0.05$  compared to Day 1). On Day 4, during the second serum-free medium incubation, the intensity stabilized at  $0.73 \pm 0.01$  AU, comparable to Day 0 but with increased variability. These findings highlight the need for refining culture conditions to sustain cell viability and support the efficiency of exosome production, particularly during repeated cycles involving serum-free media.

### Characterization of exosomes produced by 3D culture of cAD-MSCs (cEXO)

Characterization of exosomes derived from 3D cultures of cAD-MSCs (cEXO) reveals promising profiles for potential therapeutic applications. Transmission electron microscopy (TEM) analysis (Fig. 2A) confirms the typical cup-shaped morphology of cEXOs, with a size consistent with exosomal characteristics. Nanoparticle Tracking Analysis (NTA) (Fig. 2D) shows an average particle size of approximately  $81.23 \pm 7.9$  nm, within the expected range for exosomes. Zeta-potential analysis (Fig. 2B) using a Zetasizer indicates a negative surface charge of  $-19.45 \pm 0.85$  mV, suggesting moderate colloidal stability, which is ideal for therapeutic applications. Flow cytometry analysis (Fig. 2C) of the exosomal surface marker CD9 suggests the presence of exosome-like particles, confirming their biogenesis pathway. NTA reveals a high concentration of cEXOs, approximately  $1.32 \pm 0.49 \times 10^9$

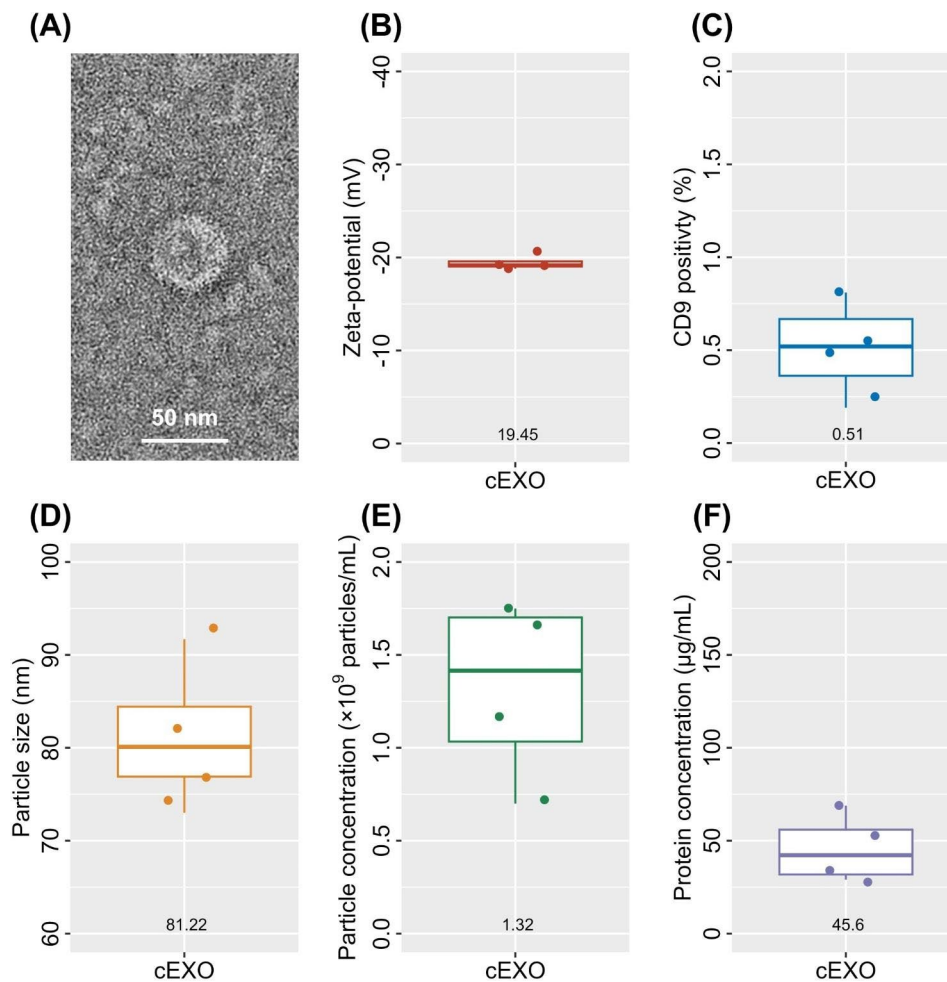


**Fig. 2** Characterization of exosomes produced by 3D culture of cAD-MSCs (cEXO). **(A)** Transmission electron microscopy (TEM) image confirms the cup-shaped morphology of cEXOs. The scale bar represents 50 nm. **(B)** Determination of zeta-potential via Zetasizer indicates negativity of cEXO surface charge. **(C)** Nanoscale flow cytometry analysis of exosomal surface marker CD9 suggests biogenesis pathway of cEXO. Nanoparticle tracking analysis (NTA) informs **(D)** particle size and **(E)** particle concentration profiles of cEXO. **(F)** Protein concentration of cEXOs quantified by fluorescence spectrophotometry reveals the purity of cEXO

particles/mL for 205 mL (Fig. 2E), indicating efficient production from the 3D culture system. The protein concentration of  $45.6 \pm 18.42 \mu\text{g/mL}$ , as measured by fluorescence spectrophotometry (Fig. 2F), implying the purity of cEXO by particle-to-protein ratio of  $2.89 \pm 1.08 \times 10^7$  particles/ $\mu\text{g}$  protein.

### Freezing storage condition preserves particle integrity and maintains the stability of cEXO

The stability of exosomes was assessed at two different temperatures ( $-20^\circ\text{C}$  and  $4^\circ\text{C}$ ) over a 30-day period. The particle size measured by NTA at  $-20^\circ\text{C}$  increased significantly from  $67.13 \pm 5.23$  nm at day 0 to  $95.48 \pm 3.09$  nm at day 15 ( $p \leq 0.01$ ) but showed no significant change between day 15 and day 30 ( $p > 0.05$ ), remaining at  $91.18 \pm 14.59$  nm at day 30 (Fig. 3A). In contrast, at  $4^\circ\text{C}$ , the particle size increased significantly between day 0 ( $67.13 \pm 5.23$  nm) and day 30 ( $80.45 \pm 6.32$  nm) ( $p \leq 0.01$ )

(Fig. 3A). The particle concentration from NTA showed no significant changes at  $-20^\circ\text{C}$  throughout the storage period ( $p > 0.05$ ), while at  $4^\circ\text{C}$ , a significant decrease in particle concentration was observed between day 0 ( $2.69 \pm 0.42 \times 10^8$  particles/mL) and day 30 ( $1.9 \pm 0.22 \times 10^8$  particles/mL) ( $p \leq 0.05$ ) (Fig. 3B). Further analysis of particle concentration using NTA (Fig. 3C) demonstrated that at  $-20^\circ\text{C}$ , exosome populations exhibited minor shifts in size distribution but retained a higher concentration compared to  $4^\circ\text{C}$ . In contrast, exosomes stored at  $4^\circ\text{C}$  showed a marked decrease in concentration, with fewer particles detected across the size range.

The particle size measured by the Zetasizer at  $-20^\circ\text{C}$  remained stable from day 0 to day 15 but increased significantly between day 15 ( $244.7 \pm 14.99$  nm) and day 30 ( $368.78 \pm 17.27$  nm) ( $p \leq 0.05$ ) (Fig. 3D). At  $4^\circ\text{C}$ , a significant increase in particle size was observed between day 0 ( $255.78 \pm 12.75$  nm) and day 30 ( $280.45 \pm 15.32$  nm)

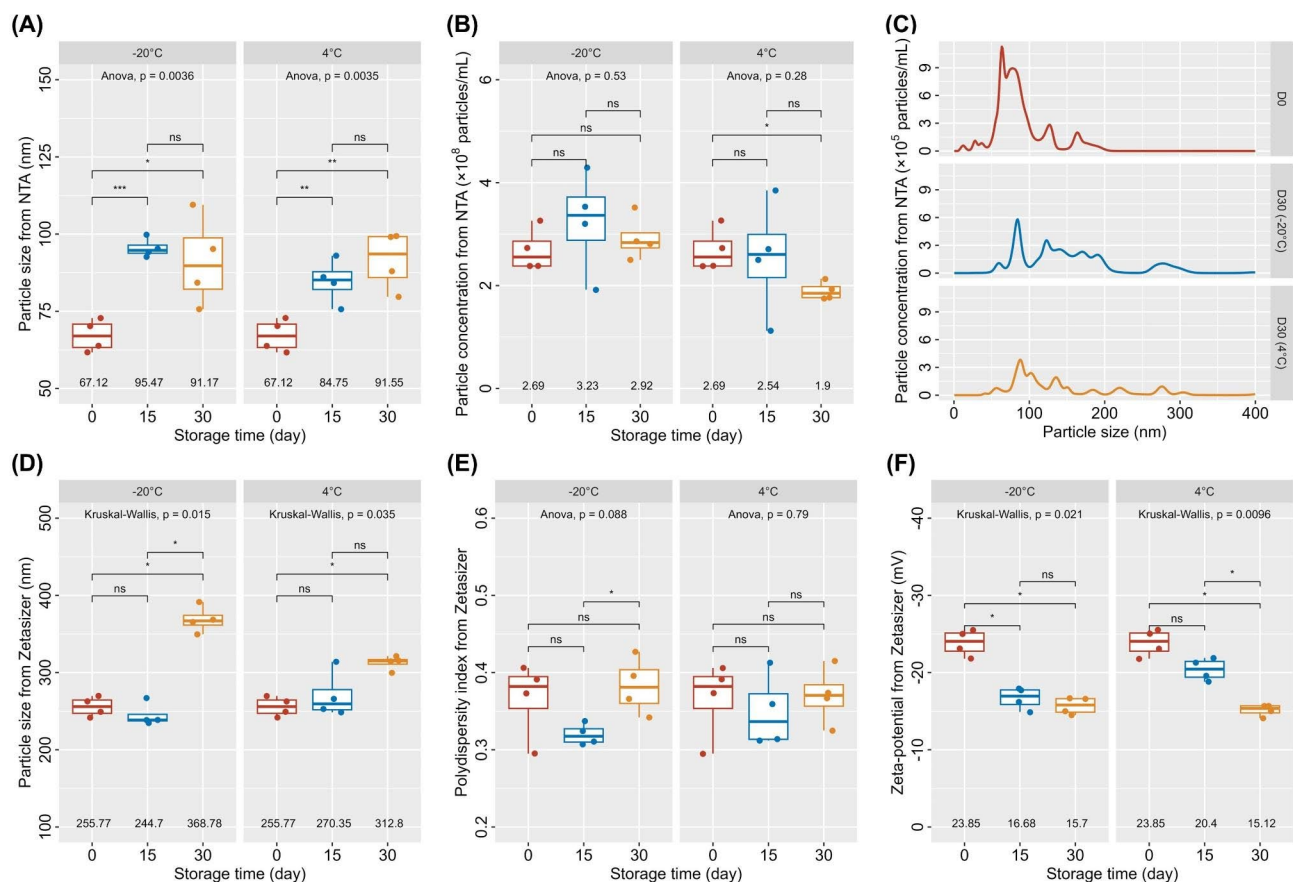


**Fig. 3** Stability study of cEXO stored under freezing ( $-20^\circ\text{C}$ ) and refrigerating ( $4^\circ\text{C}$ ) conditions. **(A)** Boxplot of particle size measured by nanoparticle tracking analysis (NTA) over the study period (0, 15, and 30 days). **(B)** Boxplot of particle concentration from NTA, showing minimal changes at  $-20^\circ\text{C}$  but a significant decrease at  $4^\circ\text{C}$  by Day 30. **(C)** Line plot illustrating particle size distribution from NTA, highlighting the shifts in particle size over time. **(D)** Boxplot of particle size measured by Zetasizer, indicating particle size stability at  $-20^\circ\text{C}$  and changes at  $4^\circ\text{C}$ . **(E)** Boxplot of polydispersity index (PDI) from Zetasizer, showing stability in particle uniformity at  $-20^\circ\text{C}$ . **(F)** Boxplot of zeta-potential from Zetasizer, demonstrating a decrease in negativity of surface charge over time, especially at  $4^\circ\text{C}$ . In all boxplots, the mean values for each group are annotated at the bottom, and global statistics are presented at the top. The bars indicate pairwise comparisons (ns; no significance or  $p > 0.05$ , \*;  $p \leq 0.05$ , \*\*;  $p \leq 0.01$ , \*\*\*;  $p \leq 0.001$ ). **Abbreviation:** cEXO; exosomes produced by 3D culture of cAD-MSCs

( $p \leq 0.05$ ). The polydispersity index (PDI) remained relatively stable at both temperatures, except for a slight but significant increase at  $-20^\circ\text{C}$  between day 15 and day 30 ( $p \leq 0.05$ ) (Fig. 3E). The zeta potential at  $-20^\circ\text{C}$  decreased significantly from  $-23.85 \pm 1.71$  mV at day 0 to  $-16.68 \pm 1.41$  mV at day 15 ( $p \leq 0.05$ ), with no significant changes thereafter (Fig. 3F). At  $4^\circ\text{C}$ , the zeta potential decreased significantly between day 0 ( $-23.85 \pm 1.71$  mV) and day 30 ( $-18.56 \pm 1.59$  mV) ( $p \leq 0.05$ ).

These findings suggest that particle size and zeta potential are more stable at  $4^\circ\text{C}$ , with fewer fluctuations compared to  $-20^\circ\text{C}$ . However, particle concentration decreased significantly over time at  $4^\circ\text{C}$ , highlighting the need for optimized storage conditions to preserve exosome integrity and functionality.

### cEXO exerts anti-inflammatory potential in LPS-induced RAW264.7 macrophage model

The anti-inflammatory assay provides a detailed analysis of cEXO's effects on RAW264.7 macrophages. Figure 4A depicts the experimental setup, where macrophages were treated with lipopolysaccharide (LPS)

to induce inflammation, followed by exposure to PBS (blank control), DEXA (dexamethasone as a positive anti-inflammatory control), or varying concentrations of cEXO. Post-treatment assays included the nitrite assay to measure nitric oxide (NO) release, a key inflammation marker, and the resazurin assay to determine cell viability.

Microscopy images (Fig. 4B) reveal distinct morphological changes in macrophages across treatments. Macrophages treated with PBS under LPS-free conditions (LPS-) displayed a small, rounded morphology characteristic of the M0 (resting) phenotype. In contrast, macrophages treated with PBS in the presence of LPS (LPS+) exhibited a larger, amoeboid morphology typical of the pro-inflammatory M1 state. DEXA treatment and cEXO exposure shifted macrophages toward a more compact, rounded morphology indicative of the anti-inflammatory M2 phenotype. Higher cEXO concentrations ( $10^6$  particles/mL) elicited a more pronounced M2-like response compared to lower concentrations.

Cytotoxicity analysis (Fig. 4C) indicates that cEXO treatment does not significantly affect macrophage viability under either LPS- or LPS+ conditions. Cell

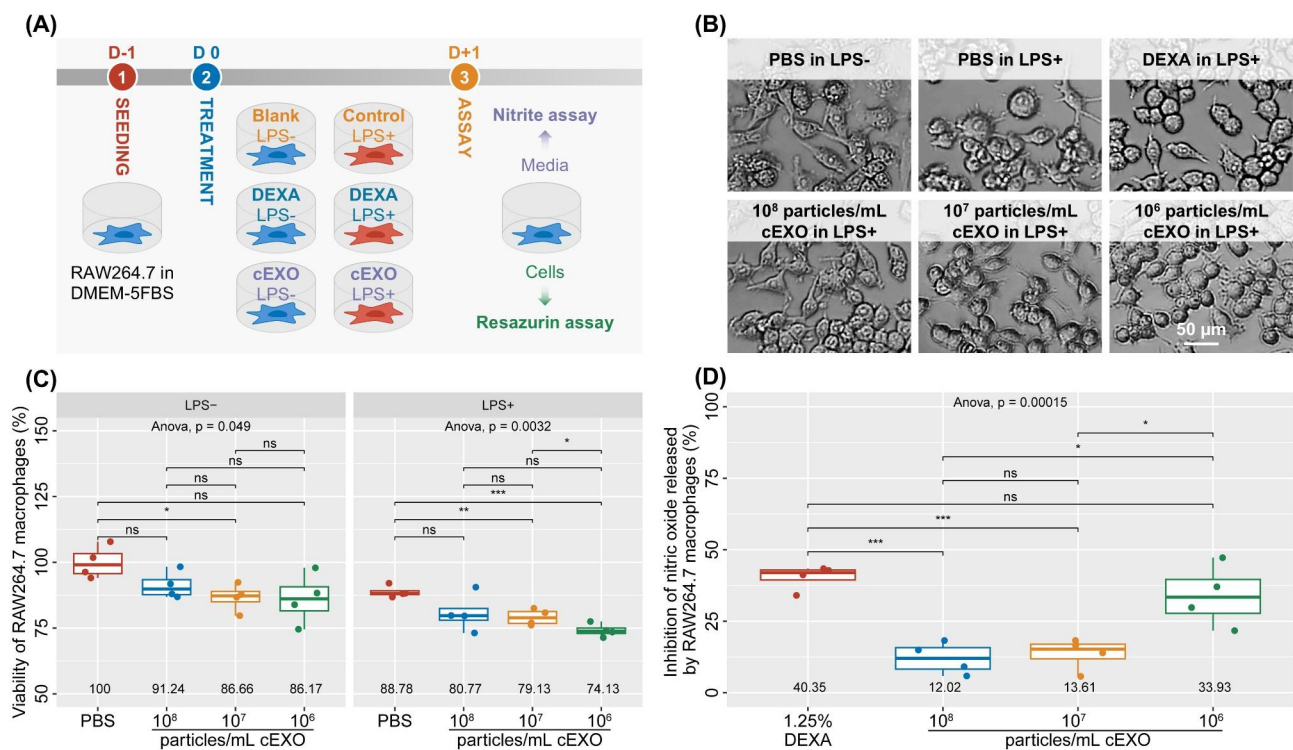


**Fig. 4** In vitro anti-inflammatory activity of cEXO. **(A)** Schematic diagram outlining the experimental design to evaluate the anti-inflammatory effects of cEXO on RAW264.7 macrophages, detailing the seeding, treatment, and assays for nitrite quantification and cell viability. **(B)** Bright-field microscopy images at 200X magnification showing the morphology of RAW264.7 macrophages under various treatment conditions. Scale bar represents 50  $\mu\text{m}$ . **(C)** Boxplot showing the viability of RAW264.7 macrophages grouped by LPS induction and treatment conditions, demonstrating the dose-dependent effect of cEXO on macrophage viability. **(D)** Boxplot illustrating the inhibition of nitric oxide production by RAW264.7 macrophages, highlighting the anti-inflammatory potential of cEXO. In all boxplots, mean values are annotated at the bottom, and global statistics are provided at the top. The bars indicate pairwise comparisons (ns; no significance or  $p > 0.05$ ; \*,  $p \leq 0.05$ ; \*\*,  $p \leq 0.01$ ; \*\*\*,  $p \leq 0.001$ ). **Abbreviation:** cEXO; exosomes produced by 3D culture of cAD-MSCs, LPS; lipopolysaccharides

viability remained above 80% across all treatments. Under LPS-free conditions, viability was highest for PBS ( $100 \pm 2.55\%$ ) and decreased slightly with increasing cEXO concentrations ( $10^8$  particles/mL:  $91.24 \pm 8.12\%$ ,  $10^7$  particles/mL:  $86.66 \pm 3.46\%$ ,  $10^6$  particles/mL:  $86.17 \pm 2.87\%$ ). Similarly, in LPS+ conditions, cell viability was  $100 \pm 2.55\%$  for PBS and  $88.78 \pm 8.12\%$ ,  $80.77 \pm 3.46\%$ , and  $79.13 \pm 2.87\%$  for  $10^8$ ,  $10^7$ , and  $10^6$  particles/mL cEXO, respectively. Significant differences were observed between PBS and  $10^7$  particles/mL cEXO under LPS-conditions ( $p \leq 0.05$ ) and between PBS and  $10^6$  particles/mL cEXO under LPS+ conditions ( $p \leq 0.001$ ), confirming that cEXO is not cytotoxic to RAW264.7 macrophages.

In the anti-inflammatory assay (Fig. 4D), NO release was significantly inhibited by DEXA ( $40.35 \pm 4.31\%$ ). cEXO treatments demonstrated a reverse dose-dependent effect, with  $10^6$  particles/mL cEXO showing the

highest inhibition ( $33.93 \pm 10.86\%$ ), followed by  $10^7$  particles/mL cEXO ( $13.61 \pm 5.57\%$ ), and  $10^8$  particles/mL cEXO ( $12.02 \pm 5.59\%$ ). Statistical analysis revealed significant differences between DEXA and  $10^8$  particles/mL cEXO ( $p \leq 0.001$ ), as well as between  $10^7$  and  $10^6$  particles/mL cEXO ( $p \leq 0.05$ ), highlighting variable anti-inflammatory efficacy across different cEXO concentrations. These results underscore cEXO's potential as a non-cytotoxic, anti-inflammatory therapeutic.

#### cEXO exhibits no cytotoxicity in 3T3-J2 fibroblasts

The cytotoxicity of cEXO was evaluated using 3T3-J2 fibroblasts treated with varying concentrations of cEXO compared to a PBS control. As illustrated in Fig. 5A, fibroblasts were seeded on Day -1, treated with PBS or cEXO on Day 0, and cell viability was assessed using the resazurin assay on Day +1. The results (Fig. 5B) indicate

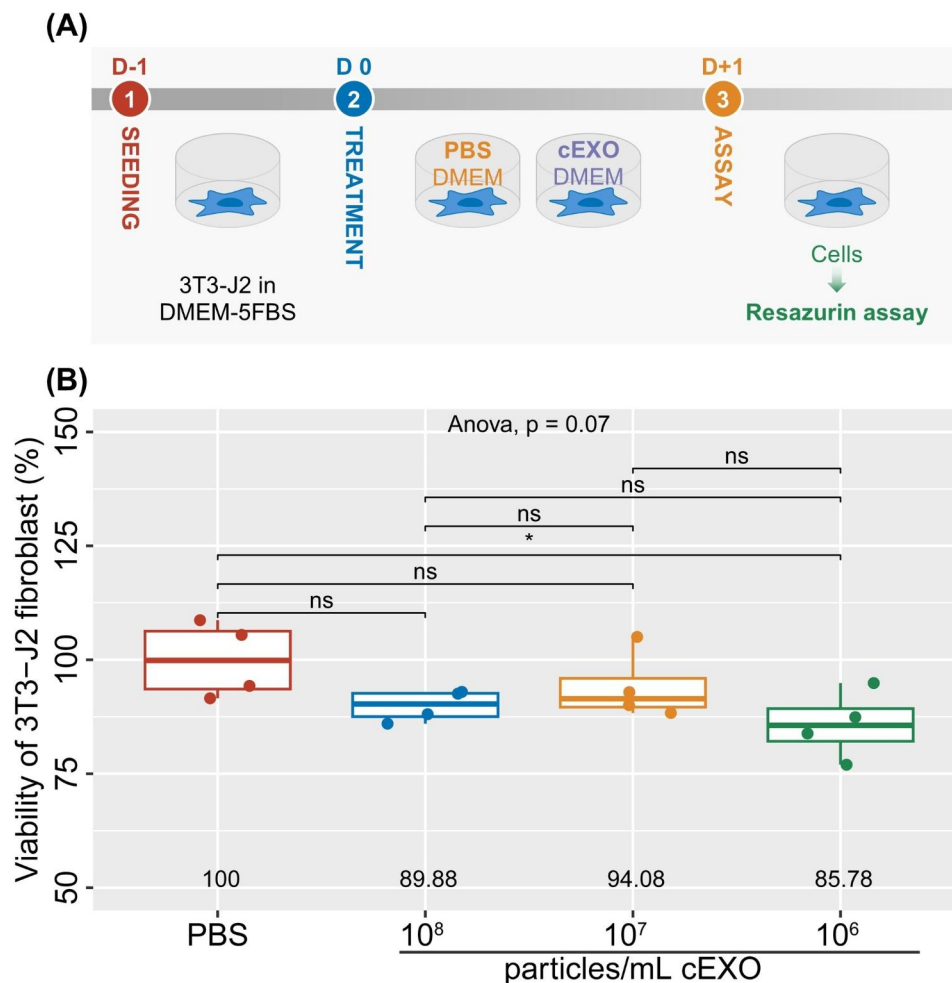


**Fig. 5** In vitro cytotoxicity of cEXO against 3T3-J2 fibroblasts. **(A)** Schematic representation of the experimental workflow, including seeding 3T3-J2 fibroblasts, treatment with varying concentrations of cEXO, and evaluation of cell viability using resazurin assay. **(B)** Boxplot displaying the viability of 3T3-J2 fibroblasts treated with cEXO, demonstrating non-cytotoxicity. In boxplots, mean values of each group were annotated at the bottom, and global statistics were stated at the top. The bars indicate pairwise comparisons (ns; no significance or  $p > 0.05$ , \*;  $p \leq 0.05$ ). **Abbreviation:** cEXO; exosomes produced by 3D culture of cAD-MSCs

that fibroblast viability remained near baseline PBS levels ( $100 \pm 8.37\%$ ), with values of  $89.88 \pm 3.42\%$  for  $10^8$  particles/mL cEXO,  $94.08 \pm 7.53\%$  for  $10^7$  particles/mL cEXO, and  $85.78 \pm 7.45\%$  for  $10^6$  particles/mL cEXO. Statistical analysis revealed no significant differences among groups (ANOVA,  $p > 0.05$ ), except for a significant reduction in viability between PBS and  $10^6$  particles/mL cEXO ( $p \leq 0.05$ ). These findings suggest that cEXO has minimal cytotoxic effects on fibroblasts, even at high concentrations, confirming its biocompatibility and supporting its potential for therapeutic applications.

### Demonstration of safety of cEXO in acute toxicity in a rodent model (ISO 10993-11)

This study evaluated the acute toxicity of exosomes produced from 3D cultures of cAD-MSCs (cEXO) in female Sprague-Dawley rats over 14 days following a single intravenous dose of  $10^9$  particles/mL cEXO via the tail vein. As illustrated in Fig. 6A, the experiment comprised

acclimatization, cEXO administration, a 14-day observation period, and organ examination. No mortality or morbidity was observed at any point, including at 24-, 48-, and 72-hour post-administration and through Day 14. Clinical evaluations showed no signs of abnormal behaviors or movements, such as tremors, convulsions, lethargy, labored breathing, diarrhea, hypersalivation, or ocular discharge.

The rats were provided with a sterilized pellet diet and reverse osmosis (RO) water ad libitum, and their food and water intake were recorded. While slight fluctuations were noted, all values remained within the expected ranges for adult rats (5–6 g/100 g body weight/day for food and 10–12 mL/100 g body weight/day for water) [12]. Detailed intake data are presented in Tables 1 and 2. Body weight monitoring, conducted at baseline, 24-, 48-, and 72-hour post-administration, as well as on Days 7 and 14, indicated trends consistent with normal growth patterns. One rat (ID1) experienced a temporary

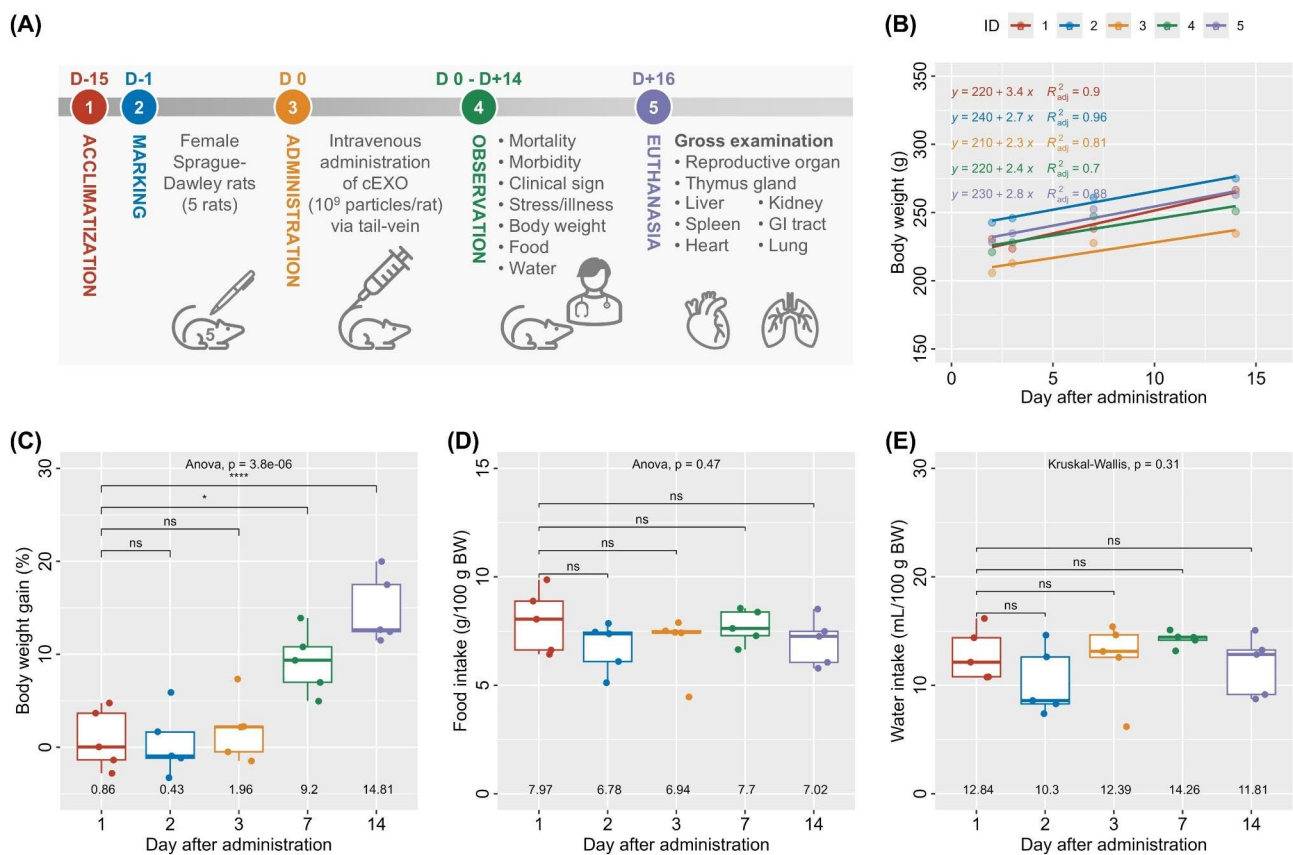


**Fig. 6** In vivo acute toxicity evaluation of cEXO in a rodent model. **(A)** Schematic diagram summarizing the acute toxicity study design in female Sprague-Dawley rats. The experiment involved acclimatization, marking, intravenous administration of cEXO, followed by a 14-day observation period. Euthanasia was conducted on day 16 for gross examination of major organs. **(B)** Body weight monitoring across the 14-day period for individual rats ( $n = 5$ ). Linear regression analysis indicated consistent weight gain trends with no adverse deviations among treatment groups. **(C)** Boxplot of body weight gain at different time points. **(D)** Food intake measurements over time showed stable dietary consumption across all rats. **(E)** Water intake measurements remained consistent throughout the observation period. In boxplots, mean values of each group were annotated at the bottom, and global statistics were stated at the top. The bars indicate pairwise comparisons (ns; no significance or  $p$ -value  $> 0.05$ , \*;  $p \leq 0.05$ , \*\*\*\*;  $p \leq 0.0001$ ). **Abbreviation:** cEXO; exosomes produced by 3D culture of cAD-MSCs, GI tract; gastrointestinal tract, ID; animal identical number, and BW; body weight

**Table 1** Daily food consumption per rat over 14 days following exosome administration

Food consumption (g/animal/day)	The days after exosome administration													
	1	2	3	4	5	6	7	8	9	10	11	12	13	14
ID 01	20.88	17.18	9.97	15.93	20.35	15.74	17.35	16.94	19.51	19.55	18.04	18.98	18.07	19.96
ID 02	23.67	19.04	18.29	16.98	20.35	15.74	17.35	16.94	19.51	19.55	18.04	18.98	18.07	19.96
ID 03	16.75	12.54	15.79	17.00	20.35	15.74	17.35	16.94	19.51	19.55	18.04	18.98	18.07	19.96
ID 04	13.95	16.30	17.99	18.01	17.70	15.73	21.14	20.15	23.37	17.52	20.17	22.08	19.53	15.20
ID 05	15.42	11.69	17.63	17.22	17.70	15.73	21.14	20.15	23.37	17.52	20.17	22.08	19.53	15.20

Note: Data presented as grams consumed per animal per day (g/animal/day)

weight decrease at 48 and 72 h, but its weight recovered from Day 4 onwards without any associated clinical abnormalities.

As shown in Fig. 6B, all rats demonstrated consistent weight gain ( $2.72 \pm 0.43$  g/day), with a significant increase of 14.81% by Day 14 (ANOVA,  $p \leq 0.0001$ ; Fig. 6C). Body weight trends for all rats are summarized in Table 3, further supporting the lack of adverse effects. Food intake (Fig. 6D) and water intake (Fig. 6E) remained stable with no significant differences ( $p > 0.05$ ), confirming that cEXO did not adversely impact appetite or hydration. At the study's conclusion, all rats were fasted overnight, euthanized, and subjected to gross necropsy. Examination revealed no abnormalities in major organs, including the liver, kidneys, spleen, gastrointestinal tract, reproductive organs, heart, lungs, and thymus gland. These results confirm the safety and non-toxicity of cEXO, supporting its potential for therapeutic applications.

## Discussion

This study demonstrates the feasibility of using a microcarrier-based 3D culture system for scalable exosome production from canine adipose-derived mesenchymal stem cells (cAD-MSCs). The microcarrier-based system has shown substantial promise in enhancing exosome yield by providing a suitable microenvironment that promotes robust MSC proliferation, similar to previous reports where 3D culture systems improved MSC expansion and exosome production [3, 13]. The approach of intermittent agitation during the seeding phase, followed by a resting period, was crucial for achieving stable cellular adhesion on the microcarriers. This methodology is consistent with earlier findings that emphasize the importance of optimizing physical parameters such as agitation and resting cycles to improve cell attachment and stability [14]. However, transitioning to serum-free media (0% FBS medium; VSCBIC-3) for exosome production introduced challenges related to cell viability. As seen in previous studies, serum-free conditions can impose metabolic stress on MSCs, leading to reduced viability and cellular stress [15, 16]. To mitigate this, optimizing the serum-free media composition or incorporating small molecules to support cellular metabolism would enhance both cell viability and exosome yield during extended culture periods [17, 18].

The characterization of exosomes, using techniques such as Transmission Electron Microscopy (TEM), revealed cup-shaped vesicles, consistent with the expected morphology for exosomes [19]. The moderate zeta potential observed indicates adequate colloidal stability, crucial for maintaining exosome dispersal and functionality, particularly in therapeutic applications [20]. Ensuring colloidal stability is essential for preserving exosome integrity during storage and enhancing their

**Table 2** Daily water consumption per rat over 14 days following exosome administration

Water consumption (mL/animal/day)	The days after exosome administration													
	1	2	3	4	5	6	7	8	9	10	11	12	13	14
ID 01	28.52	19.80	13.83	31.06	42.51	25.80	34.37	27.38	24.71	30.15	31.20	17.58	29.74	35.32
ID 02	38.79	35.45	37.86	35.96	42.51	25.80	34.37	27.38	24.71	30.15	31.20	17.58	29.74	35.32
ID 03	29.95	17.04	26.77	35.55	42.51	25.80	34.37	27.38	24.71	30.15	31.20	17.58	29.74	35.32
ID 04	23.33	27.88	33.39	39.97	27.68	25.06	35.74	31.14	27.56	22.52	35.92	34.75	30.86	22.96
ID 05	25.09	16.87	30.82	33.78	27.68	25.06	35.74	31.14	27.56	22.52	35.92	34.75	30.86	22.96

Note: Data presented as milliliters consumed per animal per day (mL/animal/day)

therapeutic efficacy. Furthermore, the particle-to-protein ratio suggested potential contamination from free proteins, a common challenge in exosome isolation, underscoring the need for further optimization of purification protocols [21, 22]. Referring to the MISEV2023 guidelines, we evaluated the quality of exosome samples by detecting CD9, a well-recognized marker of tetraspanin-enriched exosome populations, using alternative methods. While we acknowledge the necessity of including additional positive markers (e.g., CD63, CD81) and negative markers (e.g., calnexin), our efforts were limited by the unavailability of commercial anti-dog antibodies. These limitations highlight the need for more robust and comprehensive characterization approaches.

Our study provides critical insights into the stability of exosomes stored at two different temperatures (-20 °C and 4 °C) over 30 days. The observed changes in particle size, concentration, and zeta potential highlight the intricate interplay between storage conditions and exosome integrity, underscoring the need for precise temperature management. At -20 °C, significant increases in particle size measured by NTA and the Zetasizer indicate potential vesicle aggregation or fusion during freezing. These changes, particularly evident between day 0 and day 15, are consistent with reports suggesting that freezing-induced stress can cause vesicle aggregation or fusion, potentially impacting their bioactivity or vesicle leakage [23, 24]. The larger particle size measured by the Zetasizer compared to NTA is attributable to the differences in measurement principles. The Zetasizer, which uses dynamic light scattering (DLS), calculates the hydrodynamic diameter that includes the hydration shell and any associated aggregates, leading to larger size values [25]. In contrast, NTA measures individual particle movements through Brownian motion, providing a more accurate representation of vesicle size in heterogeneous populations [26]. Interestingly, particle concentration at -20 °C remained stable over time, suggesting that despite structural alterations, the number of vesicles was preserved. However, the significant reduction in zeta-potential at -20 °C suggests changes in surface charge, which could impair cellular uptake and functionality [27]. Conversely, refrigeration at 4 °C demonstrated fewer changes in particle size and zeta potential, reflecting a more stable storage condition for maintaining vesicle structure. However, the notable decline in particle concentration at 4 °C suggests that prolonged refrigeration may lead to vesicle degradation, likely due to oxidative and enzymatic activities [28, 29]. Our results emphasize that while refrigeration may better preserve exosome morphology and surface characteristics, freezing conditions require further optimization to prevent aggregation [30].

This study shows that cEXO can promote a shift from the pro-inflammatory M1 macrophage phenotype to an

**Table 3** Body weight progression and percentage gain in rats after exosome administration

Animal ID	Body weight after administration						Gain <sup>(a)</sup>	%Gain <sup>(b)</sup>
	Day 0	Day 1	Day 2	Day 3	Day 7	Day 14		
ID 01	226.87	235.17	230.60	223.52	238.16	266.58	39.71	17.50
ID 02	229.13	240.02	242.59	245.90	260.98	274.94	45.81	19.99
ID 03	208.15	208.22	205.72	212.83	227.62	234.46	26.31	12.64
ID 04	223.15	216.92	221.04	228.02	247.25	250.91	27.76	12.44
ID 05	235.89	232.69	228.22	234.75	252.38	262.98	27.09	11.48
<b>Mean ± S.D.</b>	<b>224.64 ± 10.32</b>	<b>226.60 ± 13.44</b>	<b>225.63 ± 13.57</b>	<b>229.00 ± 12.36</b>	<b>245.28 ± 12.88</b>	<b>257.97 ± 15.73</b>	<b>33.34 ± 8.88</b>	<b>14.81 ± 3.73</b>

Note: Note: Data presented as body weight measurements (grams; g) at each time point, with (a) Gain calculated as Day 14 - Day 0, and (b) %Gain as (Gain / Body weight at Day 0) × 100

M2-like anti-inflammatory state. Exosomes derived from mesenchymal stem cells (MSCs) have been shown to modulate macrophage polarization by reducing inflammatory markers and enhancing anti-inflammatory pathways [31, 32]. Additionally, the ability of cEXO treatments to maintain high cell viability under LPS-induced inflammatory stress is in agreement with studies that confirm MSC-derived exosomes preserve cell health even under inflammatory conditions [33, 34]. Lipopolysaccharide (LPS), a component of the outer membrane of Gram-negative bacteria, is a potent activator of the innate immune system. It induces inflammation by stimulating macrophages to produce pro-inflammatory cytokines and nitric oxide (NO) via the TLR4/NF-κB signaling pathway, as demonstrated in various studies on LPS-induced immune responses [35, 36]. This cascade is widely recognized as a robust model for assessing the bioactivity of anti-inflammatory agents, including exosomes derived from canine adipose-derived mesenchymal stem cells (cEXO). In this study, cEXO significantly reduced LPS-induced NO production and modulated macrophage polarization, shifting them from a pro-inflammatory M1 phenotype to an anti-inflammatory M2 phenotype [37]. These effects are likely mediated by exosomal cargo, including miRNAs, proteins, and lipids, which can interact with molecular targets downstream of TLR4, such as NF-κB, to suppress its activation [38, 39]. Moreover, cEXO could enhance anti-inflammatory mediators like IL-10, promoting a shift from pro-inflammatory to anti-inflammatory macrophage phenotypes [40]. These findings underscore the therapeutic potential of cEXO as modulators of immune responses and promising candidates for managing inflammation-related conditions.

The observed reverse dose-dependent effect, where lower exosome concentrations demonstrated greater anti-inflammatory activity than higher concentrations, aligns with findings in similar biological contexts. For instance, the anti-inflammatory effects of rhoifolin in a carrageenin-induced rat paw edema model revealed a reverse dose-dependent pattern, with the greatest anti-oxidant and anti-inflammatory effects observed at the

lowest dose tested. This phenomenon was attributed to optimal engagement of anti-inflammatory pathways at lower doses, as higher doses diminished the total anti-oxidant capacity and modulated cytokine release sub-optimally [41]. Similarly, the dose-dependent effects observed in neuromuscular-blocking agents and their reversal by neostigmine emphasize the potential for overdosing to introduce adverse effects due to saturation or feedback mechanisms. At higher doses, receptor or enzyme targets may become oversaturated, reducing efficacy and increasing risks, whereas optimal dosing strategies significantly mitigated complications [42]. This concept also applies to digoxin-specific antibody interactions, where stoichiometric Fab: digoxin ratios reversed inhibition efficiently, but excessive antibody doses failed to enhance efficacy and suggested receptor saturation or off-target effects [43]. In the context of exosome-mediated anti-inflammatory effects, higher concentrations of exosomes could saturate receptors or induce feedback inhibition, suppressing signaling efficacy. Additionally, higher doses may lead to cargo competition within recipient cells, interfering with the intracellular processing of bioactive molecules. Conversely, lower concentrations are likely to achieve a balanced interaction, optimizing signal modulation without overwhelming cellular pathways. These findings highlight the need for precise dose optimization in exosome-based therapies to ensure maximum therapeutic efficacy while avoiding the potential drawbacks associated with higher doses.

Exosomes derived from MSCs are inherently biocompatible due to their natural origin and low immunogenic properties [44, 45]. This supports their potential for regenerative medicine applications, including the observed lack of cytotoxicity in fibroblasts, indicating that cEXO can be safely applied in regenerative medicine without compromising fibroblast function [46, 47]. The use of resazurin as a viability assay, measuring mitochondrial activity, further confirms the lack of cytotoxicity, as mitochondrial health is a reliable indicator of overall cell viability [48, 49]. Moreover, the results of the in vivo acute toxicity test show that the administration of cEXO did not result in metabolic disturbances or systemic

toxicity. Consistent body weight gain across all rats suggests that the exosome treatment did not induce adverse effects on overall health [50, 51]. Gross necropsy findings, showing no abnormalities in major organs, further support the conclusion that cEXO does not induce overt tissue damage or histopathological changes [52].

This study highlights the therapeutic potential of exosomes derived from 3D cultures of canine adipose-derived mesenchymal stem cells (cAD-MSCs); however, several limitations should be addressed. Firstly, while exosomes were characterized using CD9 as a marker of exosomal biogenesis, additional markers such as CD63, CD81, and TSG101 should be included to confirm exosome purity and eliminate potential contamination from other extracellular vesicles, as recommended by the MISEV guidelines [53, 54]. A more rigorous marker-based characterization would enhance the reproducibility and reliability of the findings. Secondly, the small sample size and variability in donor-derived cAD-MSCs may limit reproducibility and generalizability [55]. Expanding the study to include a larger and more diverse pool of donors would improve the robustness of the results. Thirdly, while the stability of cEXO was evaluated under freezing and refrigeration conditions, future research should explore strategies for room-temperature suspension formulations. Stabilizers such as trehalose or polyethylene glycol (PEG) could prevent aggregation and maintain exosome integrity, making them more practical for clinical applications, particularly in resource-limited settings [56].

## Conclusion

This research proves the feasibility and efficacy of producing exosomes from cAD-MSCs (cEXO) using a microcarrier-based 3D culture system. The study shows that cEXO exhibit stable physicochemical properties, low cytotoxicity, and significant anti-inflammatory potential, making them promising candidates for therapeutic applications. Optimized culture conditions enabled efficient exosome production, though challenges such as maintaining cell viability during serum-free medium cycles were noted. Stability studies revealed that cEXO maintain their integrity and functionality better under frozen conditions compared to refrigeration. In vitro assays confirmed ability of cEXO to modulate macrophage responses and reduce nitric oxide release, indicative of anti-inflammatory activity. Furthermore, acute toxicity evaluation in a rodent model revealed no adverse effects, with consistent growth, stable food and water intake, and no abnormalities in major organs. Collectively, these findings suggest that cEXO are safe and effective, supporting their potential for future clinical translation in inflammatory and regenerative therapies.

## Methods

### Isolation and expansion of cAD-MSCs

Adipose tissue was collected from a 5-year-old female German Shepherd (33.6 kg) at the Small Animal Teaching Hospital, Faculty of Veterinary Science, Chulalongkorn University, Thailand. The procedure adhered to ethical standards outlined by the Institutional Animal Care and Use Committee (IACUC) of the Faculty of Veterinary Science, Chulalongkorn University, Thailand, and was approved under Animal Use Protocol 2231041. Since the dog was privately owned, informed consent was obtained from the owner prior to tissue collection. The tissue was minced, treated with the Cell Recovery Solution, a nonenzymatic proprietary solution designed to recover cells while preserving their integrity, and filtered through a 70  $\mu\text{m}$  strainer. The isolated cells were cultured in expansion medium (DMEM-10FBS), consisting of Dulbecco's Modified Eagle Medium (DMEM; Thermo Fisher Scientific, USA) supplemented with 10% fetal bovine serum (FBS; Thermo Fisher Scientific, USA), under standard conditions of 37 °C, 5% CO<sub>2</sub>, and 95% relative humidity. Subculturing was performed when the cells reached 80–90% confluence. Cells from passages 3–5 were confirmed as mesenchymal stem cells according to the International Society for Cellular Therapy (ISCT) standards [55]. Characterization included morphological observation (fibroblastic-like shape), surface marker analysis (CD29+, CD44+, CD90+, and CD45-), and mRNA expression profiling for stemness markers (*Oct4* and *Rex1*) and the proliferation marker (*Ki-67*), as detailed in a previous study [57].

The trilineage differentiation potential of cAD-MSCs was assessed through adipogenic, osteogenic, and chondrogenic protocols. Adipogenesis was confirmed by intracellular lipid droplet formation visualized with Oil Red O staining and by mRNA expression of adipogenic markers (*Lep* and *Lpl*). Osteogenesis was validated by extracellular matrix mineralization using Alizarin Red S staining and by mRNA expression of osteogenic markers (*Ocn* and *Runx2*). Chondrogenesis was demonstrated by glycosaminoglycan formation detected with Alcian Blue staining and by mRNA expression of chondrogenic markers (*Col2a1* and *Sox9*). These findings confirmed the trilineage differentiation capability of the isolated cAD-MSCs, validating their stem cell identity and functional potential, as detailed in an earlier work [57].

### Production and characterization of exosomes from cAD-MSCs by 3D culture

Anti-inflammatory exosomes were derived from canine adipose-derived mesenchymal stem cells (cAD-MSCs) cultured in a three-dimensional (3D) environment using polystyrene microcarriers (Corning, USA), as illustrated in Fig. 1A. Exosome production was performed

in a 250-mL glass spinner flask (Corning, USA) over an 8-day culture period. Initially, cAD-MSCs were seeded at a density of 20,000 cells/cm<sup>2</sup>, with microcarrier loading at 4.8 cm<sup>2</sup>/mL in serum-containing media (180 mL; DMEM-10FBS). Agitation cycles of 5 min followed by 25 min of resting were conducted at 75 rpm, repeated six times during seeding [58]. After a 21-hour resting phase to promote cell attachment, the cell expansion phase lasted for 3 days under continuous agitation at 75 rpm.

Following cell expansion, the medium was replaced with in-house serum-free defined medium (0% FBS medium; VSCBIC-3) for 24 h, and conditioned media were collected (165 mL) on Day 1. To remove cell debris and microvesicles, the media were filtered through a 0.22- $\mu$ m PES filter (Membrane Solutions, USA) and stored at 4–6 °C for further processing [59]. After a 2-day refreshment period with expansion media, the medium was replaced again with VSCBIC-3 on Day 3. Following 24 h of preconditioning, conditioned media (165 mL) were collected on Day 4, filtered through a 0.22- $\mu$ m PES filter, and stored similarly.

Conditioned media collected on Days 1 and 4 were pooled (330 mL) and processed using tangential flow filtration (TFF) with a 100-kDa cassette (Merck, Germany). To preserve exosome integrity, samples were maintained at 4–6 °C or on ice throughout purification. The pooled media were concentrated to 5 mL (66X concentration) using TFF and subjected to buffer exchange with Dulbecco's phosphate-buffered saline (DPBS; Gibco, USA) to achieve a final volume of 205 mL (40X buffer addition). The exosome solution (cEXO) was sterilized using a 0.22- $\mu$ m PVDF syringe filter (Merck, Germany), aliquoted, and stored at -20 °C. Prior to use or analysis, the cEXO was thawed in a 37 °C water bath for 30 s.

The cEXO was comprehensively characterized for morphology, surface markers, stability, particle size, concentration, and protein content. Transmission electron microscopy (TEM) confirmed the cup-shaped morphology of the exosomes. For this, 10-fold diluted samples were stained with 2% uranyl acetate and visualized using a Talos F200X microscope (Thermo Fisher Scientific, USA) [60]. Nanoscale flow cytometry validated the presence of CD9, a well-recognized exosomal surface marker [61]. Samples were labeled with Exobrite™ 410/450 conjugated anti-CD9 antibody and analyzed using a DxFLEX flow cytometer (Beckman Coulter, USA), with fluorescence intensity at 450 nm confirming CD9 positivity.

Zeta-potential analysis was performed using a Zetasizer Nano ZS (Malvern Instruments, UK) to evaluate surface charge and colloidal stability [62]. For this, samples were diluted tenfold in PBS. Protein concentrations were quantified using a Qubit™ Protein Assay Kit (Invitrogen, USA), where denatured samples (75 °C for 10 min)

were mixed with Qubit™ working solution and measured with a Qubit™ 3.0 Fluorometer [63].

Nanoparticle tracking analysis (NTA) was conducted using a NanoSight NS300 system (Malvern Panalytical, UK). Tenfold diluted samples were analyzed for particle size and concentration using the Stokes-Einstein equation, with particle movement recorded in 60-second videos [64]. The particle-to-protein ratio was calculated to assess sample purity.

#### **Stability study of cEXO under freezing and refrigerating conditions**

For the stability study of cEXO, 200  $\mu$ L of exosome samples were stored in amber glass vials sealed with butyl rubber stoppers and flip-off caps to protect them from light and contamination. The samples were stored at -20 °C and 4 °C for 30 days, with evaluations conducted at 0, 15, and 30 days to assess their physicochemical properties. Key parameters analyzed included particle size, polydispersity index (PDI), and zeta-potential using Zetasizer Nano ZS. Nanoparticle tracking analysis (NTA) using Nanosight NS300 was employed to determine particle size and concentration, providing insights into vesicle integrity and abundance over time. The characterization protocol is stated in the section below.

#### **In vitro anti-inflammatory activity of cEXO in LPS-induced RAW264.7 macrophage model**

The in vitro anti-inflammatory activity of cEXO from cAD-MSCs was evaluated following established protocols [37, 65], using LPS-stimulated RAW264.7 macrophages. Cryopreserved RAW264.7 cells (passage 9, ATCC, USA) were expanded and seeded in a T-75 flask, then plated at a density of 10<sup>5</sup> cells/well in a 96-well plate. After 24 h, the media were replaced with either LPS-containing media (1,000 ng/mL) or LPS-free media. Various treatments were applied, including cEXO (10<sup>6</sup> – 10<sup>8</sup> particles/mL), a positive control (1.25  $\mu$ g/mL dexamethasone; Bukalo Trading, Thailand), and a negative control (PBS; Sigma-Aldrich, USA). Following an 18-hour co-incubation, nitrite release in the conditioned media was measured using the Griess reagent assay. Briefly, 10  $\mu$ L of Griess reagent (Biotium, USA), 65  $\mu$ L of deionized water, and 75  $\mu$ L of conditioned media were mixed and incubated at room temperature for 30 min in the dark. Absorbance at 570 nm (A<sub>570</sub>) was measured using a microplate reader (Thermo Fisher Scientific, USA).

To calculate nitric oxide inhibition (NOI; %) as anti-inflammatory activity of cEXO, the A<sub>570</sub> from nitrite assay were divided by the SA<sub>570</sub> from the resazurin assay mentioned in the section “Cell viability determination” for cellular metabolism normalization. After blank correction (medium), the data from LPS-treated samples were subtracted from those of non-LPS-treated samples

[65]. the absorbance of the LPS+ group was subtracted from the LPS- group, and the resulting value was divided by that of the negative control and multiplied by 100. Cell morphology after co-incubation was observed using an Eclipse Ti2 inverted brightfield microscope (Nikon, Japan) at 200X magnification.

#### **In vitro cytotoxicity against 3T3-J2 fibroblast of cEXO**

The in vitro cytotoxicity of cEXO against 3T3-J2 fibroblasts was evaluated using a resazurin-based cell viability assay as visualized in Fig. 5A. Cells were seeded at 4,000 cells/well in a 96-well plate and incubated at 37 °C for 24 h before treatment. cEXO samples ( $10^6 - 10^8$  particles/mL) were diluted in PBS, while serum-free DMEM was used as the treatment medium. Positive (5% FBS) and negative (PBS) controls were included. After 24 h of treatment at 37 °C, the media were replaced with a 15 µg/mL resazurin solution prepared in 5% FBS DMEM, and plates were incubated for 3 h. The cell viability (CV; %) was obtained as described in the section “Cell viability determination”. Cell morphology was monitored by employing an Eclipse Ti2 inverted brightfield microscope (Nikon, Japan) with differential interference contrast objective lens at 100X magnification.

#### **In vivo study for acute toxicity evaluation of cEXO in rodent model**

According to ISO 10993-11 (2017) guidelines for acute toxicity testing in laboratory animals, five female Jcl: SD rats, aged 8 weeks, were approved for use by the Naresuan University Institutional Animal Care and Use Committee (NU-ACUC), with approval code NU-TS660302-02. The rats were housed in an AAALACi-accredited and GLP-compliant facility, undergoing a 7-day quarantine and an additional 7-day acclimatization period before the experiment. They were kept in sterile filter-top cages under controlled conditions, with a temperature of  $22 \pm 3$  °C and relative humidity of 30–70%, regulated by an HVAC system. Environmental conditions were recorded throughout the study, and the rats were provided sterilized pellet food and filtered water via a reverse osmosis system *ad libitum*.

After acclimatization, the rats underwent health checks and weight measurements before the experiment. Exosomes were administered via the tail vein at a concentration of  $10^9$  particles/mL, with a maximum volume of 40 mL/kg BW and an infusion rate not exceeding 1 mL/min. Following administration, the rats were observed for clinical signs and behavior at 24, 48, and 72 h and then monitored daily for 14 days. Body weights, food intake, and water consumption were recorded daily. If a rat exhibited a body weight reduction exceeding 20% or died within the first 24 h, data on mortality and morbidity were documented.

At the end of the experiment, if no rats died or exhibited imminent death, they were fasted overnight before being euthanized by intraperitoneal injection of Thiopental at a dose of 150 mg/kg. Death was confirmed before conducting a necropsy to examine internal organs, including the liver, kidneys, spleen, gastrointestinal tract, reproductive organs, heart, lungs, and thymus gland. Any abnormalities observed were documented and considered for further histopathological examination. This study was conducted to evaluate the safety of exosomes following international standards.

#### **Cell viability determination**

The viability of cells cultured in 96-well plate were assessed using a resazurin assay. After discarding the conditioned media, 15 µg/mL resazurin reagent (Sigma-Aldrich, USA) in DMEM-5FBS was added, and cells were incubated for 3 h. Absorbance at 570 nm (A570) and 620 nm (A620) was measured using a microplate reader (Thermo Fisher Scientific, USA). Blank subtractions were executed to obtain subtracted absorption of A570 (SA570) and A620 (SA620). The resazurin reduction (RZR; %) was corrected using a dual-wavelength spectrophotometric approach as described elsewhere [49]. Cell viability (CV; %) was calculated by dividing the RZR of the sample by that of the negative control (PBS) and multiplying by 100.

#### **Confocal laser scanning microscopy (CLSM)**

Confocal laser scanning microscopy (CLSM) was conducted using an Eclipse Ti2 inverted microscope (Nikon, Japan) to observe cells on microcarriers with live-dead staining. Live cells were stained green with Calcein AM (Sigma-Aldrich, USA), while dead cells were stained red with Propidium Iodide (PI; Sigma-Aldrich, USA), and microcarriers were visualized in blue. Imaging was performed at 200X magnification with a Z-stack configuration, capturing 29 stacks at 5 µm intervals to create a comprehensive three-dimensional view. Quantitative analysis was based on normalized calcein fluorescent intensity, calculated as the mean green channel intensity from all stacks divided by the mean blue channel intensity from all stacks. This method provided detailed insights into cell viability and attachment dynamics on microcarriers across various culture phases.

#### **Statistical analysis and visualization**

Data are presented as mean  $\pm$  standard error of the mean (SEM). For parametric datasets, the t-test was used to compare two groups, and one-way analysis of variance (ANOVA) was applied for multiple groups. Non-parametric datasets were analyzed using the Wilcoxon test for two groups and the Kruskal-Wallis test for multiple groups. The Shapiro-Wilk test was performed to assess

the normality of the datasets. Statistical significance was set at a 95% confidence interval. Data visualization and statistical analyses were conducted using R software (R Core Team, 2023), with the *ggboxplot()* function from the *ggpubr* package (version 0.6.0). Linear regression analysis was performed with the *ggplot()* function from the *ggplot2* package (version 3.4.2).

#### Abbreviations

MSC	Mesenchymal stem cell
cAD-MSC	Canine adipose-derived mesenchymal stem cell
3D	Three dimensions
cEXO	Exosomes produced from 3D culture of cAD-MSC
AU	Arbitrary unit
CD	Cluster of differentiation
VSCBIC-3	In-house serum-free defined medium
NTA	Nanoparticle tracking analysis
LPS	Lipopolysaccharide
LPS-	Non-LPS-induced condition
LPS+	LPS-induced condition
NO	Nitric oxide
NOI	Nitric oxide inhibition
PBS	Phosphate buffered saline
DEXA	Dexamethasone
ISCT	International Society for Cellular Therapy
TEM	Transmission electron microscope
IACUC	Institutional Animal Care and Use Committee
FBS	Fetal bovine serum
UV	Ultraviolet
kDa	Kilo Dalton
PDVF	Polyvinylidene fluoride
sCMOS	Scientific complementary metal-oxide-semiconductor
RZR	Resazurin reduction
SEM	Standard error of the mean
ANOVA	One-way analysis of variance
AAALACI	Association for Assessment and Accreditation of Laboratory Animal Care International
GLP	Good Laboratory Practice
HVAC System	Heating Ventilation and Air Conditioning System
ISO	International Organization for Standardization
BW	Body weight

#### Acknowledgements

The authors would like to express their gratitude to the Veterinary Stem Cell and Bioengineering Innovation Center (VSCBIC) (<http://www.cuvscbic.com>), Faculty of Veterinary Science, Chulalongkorn University, for their support in providing research facilities. The author acknowledges the use of ChatGPT-4o, a large language model, in generating and refining content for this submission. The author assumes full responsibility for the content produced with the assistance of ChatGPT-4o and appreciates the potential of language models in enhancing scientific writing and knowledge dissemination.

#### Author contributions

A.T and S.O. contributed equally to this work in terms of study design, experimentation, data analysis, and manuscript writing. P.S., W.R., P.S., D.N.N., T.O., H.E., and C.S. were involved in the study design and provided critical revisions to the manuscript. All authors have read and approved the final manuscript.

#### Funding

This research is supported by the 90th Anniversary of Chulalongkorn University, Rachadapisek Sompote Fund. In addition, this research project is supported by the Second Century Fund (C2F), Chulalongkorn University, and the scholarship from Chulalongkorn University, The Second Century Fund (C2F) is acknowledged. Furthermore, this research is funded by Thailand Science Research and Innovation Fund Chulalongkorn University (FOOD66310024). The funders had no role in the conceptualization, design, data collection, analysis, decision to publish, or preparation of the manuscript.

#### Data availability

The datasets used and/or analyzed during the current study are available from the corresponding author on reasonable request.

#### Declarations

##### Ethics approval and consent to participate

This study follows the ARRIVE guidelines and adheres to ethical standards established by the Institutional Animal Care and Use Committee (IACUC) of the Faculty of Veterinary Science, Chulalongkorn University, Thailand. The IACUC of the Faculty of Veterinary Science, Chulalongkorn University provided approval for the collection of adipose under Animal Use Protocol 2231041. This committee is not directly affiliated with the authors, ensuring an unbiased and objective review process. Adipose tissue was collected from a privately owned animal with the informed consent of the owner prior to the procedure. In addition, this study was conducted in accordance with the ISO 10993-11 (2017) guidelines for acute systemic toxicity testing in laboratory animals. Ethical approval was granted by the Naresuan University Institutional Animal Care and Use Committee (NU-ACUC), with approval code No. NU-TS660302-02. This committee also operates independently of the authors. The research was carried out in a facility accredited by the Association for Assessment and Accreditation of Laboratory Animal Care International (AAALACI) and certified as a GLP Compliant Test Facility, ensuring compliance with international standards for animal care and research practices.

##### Consent for publication

Not applicable.

##### Competing interests

The authors declare no competing interests.

##### Author details

<sup>1</sup>Department of Social and Administrative Pharmacy, Faculty of Pharmaceutical Sciences, Chulalongkorn University, Bangkok 10330, Thailand

<sup>2</sup>Second Century Fund (C2F), Chulalongkorn University for Post-doctoral Fellowship, Chulalongkorn University, Bangkok 10330, Thailand

<sup>3</sup>Center of Excellence for Veterinary Clinical Stem Cells and Bioengineering, Faculty of Veterinary Science, Chulalongkorn University, Bangkok 10330, Thailand

<sup>4</sup>Veterinary Stem Cell and Bioengineering Innovation Center (VSCBIC), Veterinary Pharmacology, Stem Cell Research Laboratory, Faculty of Veterinary Science, Chulalongkorn University, Bangkok 10330, Thailand

<sup>5</sup>Department of Pharmacology, Faculty of Veterinary Science, Chulalongkorn University, Bangkok 10330, Thailand

<sup>6</sup>Center of Excellence in Systems Biology, Faculty of Medicine, Chulalongkorn University, Bangkok 10330, Thailand

<sup>7</sup>Center of Excellence for Dental Stem Cell Biology, Faculty of Dentistry, Chulalongkorn University, Bangkok 10330, Thailand

<sup>8</sup>Department of Physiology, Faculty of Dentistry, Chulalongkorn University, Bangkok 10330, Thailand

<sup>9</sup>Department of Anatomy, Faculty of Dentistry, Chulalongkorn University, Bangkok 10330, Thailand

<sup>10</sup>Dental Stem Cell Biology Research Unit, Faculty of Dentistry, Chulalongkorn University, Bangkok 10330, Thailand

<sup>11</sup>Center of Excellence in Regenerative Dentistry (CERD), Faculty of Dentistry, Chulalongkorn University, Bangkok 10330, Thailand

<sup>12</sup>Center for Advanced Stem Cell and Regenerative Research, Division of Molecular and Regenerative Prosthodontics, Tohoku University Graduate School of Dentistry, Sendai 980-8575, Japan

Received: 21 November 2024 / Accepted: 24 January 2025

Published online: 20 February 2025

#### References

1. Suh JH, Joo HS, Hong EB, Lee HJ, Lee JM. Therapeutic application of exosomes in inflammatory diseases. *Int J Mol Sci.* 2021;22.

2. Xiong Y, Song J, Huang X, Pan Z, Goldbrunner R, Stavrinou L et al. Exosomes derived from mesenchymal stem cells: novel effects in the treatment of ischemic stroke. *Front Neurosci*. 2022;16.
3. Cao J, Wang B, Tang T, Lv L, Ding Z, Li Z et al. Three-dimensional culture of MSCs produces exosomes with improved yield and enhanced therapeutic efficacy for cisplatin-induced acute kidney injury. *Stem Cell Res Ther*. 2020;11.
4. Zhang Y, Chen J, Fu H, Kuang S, He F, Zhang M et al. Exosomes derived from 3D-cultured MSCs improve therapeutic effects in periodontitis and experimental colitis and restore the Th17 cell/Treg balance in inflamed periodontium. *Int J Oral Sci*. 2021;13.
5. Haraszti RA, Miller R, Stoppato M, Sere YY, Coles A, Didiot MC et al. Exosomes produced from 3D cultures of MSCs by tangential flow filtration show higher yield and improved activity. *Mol Ther*. 2018;26.
6. Lee SY, Lee JW. 3D spheroid cultures of stem cells and exosome applications for cartilage repair. *Life*. 2022;12.
7. Yan L, Li D, Li S, Jiao Li J, Du G, Liu H, et al. Exosomes derived from 3D-cultured MSCs alleviate knee osteoarthritis by promoting M2 macrophage polarization through miR-365a-5p and inhibiting TLR2/Myd88/NF- $\kappa$ B pathway. *Chem Eng J*. 2024;497:154432.
8. Chen Y, Li J, Ma B, Li N, Wang S, Sun Z et al. MSC-derived exosomes promote recovery from traumatic brain injury via microglia/macrophages in rat. *Aging*. 2020;12.
9. Wright A, Snyder OL, Christenson LK, He H, Weiss ML. Effect of pre-processing storage condition of cell culture-conditioned medium on extracellular vesicles derived from human umbilical cord-derived mesenchymal stromal cells. *Int J Mol Sci*. 2022;23.
10. Karami P, Stampoultzis T, Guo Y, Pioletti DP. A guide to preclinical evaluation of hydrogel-based devices for treatment of cartilage lesions. *Acta Biomater*. 2023;158.
11. Lee KW, Chan LK, Hung LC, Phoebe LK, Park Y, Yi K-H. Clinical applications of exosomes: a critical review. *Int J Mol Sci*. 2024;25.
12. Colby LA, Nowland MH, Kennedy LH. Clinical laboratory animal medicine: An introduction, 5th edition. Wiley-Blackwell; 2019.
13. Koh B, Sulaiman N, Fauzi MB, Law JX, Ng MH, Idrus RBH et al. Three dimensional microcarrier system in mesenchymal stem cell culture: a systematic review. *Cell Bioscience*. 2020;10.
14. Ebrahimian A, Schalk M, Dürkop M, Maurer M, Bliem R, Kühnel H. Parameter optimization and capacitance-based monitoring of in situ cell detachment in microcarrier cultures. *Processes*. 2024;12.
15. Abdeen SH, Abdeen AM, El-Enshasy HA, El Shereef AA. HeLa-S3 cell growth conditions in serum-free medium and adaptability for proliferation in suspension culture. *J Biol Sci*. 2011;11.
16. Caneparo C, Chabaud S, Fradette J, Bolduc S. Evaluation of a serum-free medium for human epithelial and stromal cell culture. *Int J Mol Sci*. 2022;23.
17. Iqbal Z, Rehman K, Mahmood A, Shabbir M, Liang Y, Duan L, et al. Exosome for mRNA delivery: strategies and therapeutic applications. *J Nanobiotechnol*. 2024;22:395.
18. Chen Y-F, Luh F, Ho Y-S, Yen Y. Exosomes. A review of biologic function, diagnostic and targeted therapy applications, and clinical trials. *J Biomed Sci*. 2024;31:67.
19. Chernyshev VS, Rachamadugu R, Tseng YH, Belnap DM, Jia Y, Branch KJ et al. Size and shape characterization of hydrated and desiccated exosomes. *Anal Bioanal Chem*. 2015;407.
20. Midekessa G, Godakumara K, Ord J, Viil J, Lättেকivi F, Dissanayake K et al. Zeta potential of extracellular vesicles: toward understanding the attributes that determine colloidal stability. *ACS Omega*. 2020;5.
21. Ekström K, Crescitelli R, Pétursson Hl, Johansson J, Lässer C, Bagge RO. Characterization of surface markers on extracellular vesicles isolated from lymphatic exudate from patients with breast cancer. *BMC Cancer*. 2022;22.
22. Yang Y, Wang Y, Wei S, Zhou C, Yu J, Wang G et al. Extracellular vesicles isolated by size-exclusion chromatography present suitability for RNomics analysis in plasma. *J Transl Med*. 2021;19.
23. Risselada HJ, Marrink SJ. The freezing process of small lipid vesicles at molecular resolution. *Soft Matter*. 2009;5.
24. Shi S, Fan H, Hoernke M. Leaky membrane fusion: an ambivalent effect induced by antimicrobial polycations. *Nanoscale Adv*. 2022;4.
25. Gollwitzer C, Bartczak D, Goenaga-Infante H, Kestens V, Krumrey M, Minelli C et al. A comparison of techniques for size measurement of nanoparticles in cell culture medium. *Anal Methods*. 2016;8.
26. Filipe V, Hawe A, Jiskoot W. Critical evaluation of nanoparticle tracking analysis (NTA) by NanoSight for the measurement of nanoparticles and protein aggregates. *Pharm Res*. 2010;27.
27. Öztürk K, Kaplan M, Çaliş S. Effects of nanoparticle size, shape, and Zeta potential on drug delivery. *Int J Pharm*. 2024;666:124799.
28. Ahmadian S, Jafari N, Tamadon A, Ghaffarzadeh A, Rahbarghazi R, Mahdipour M. Different storage and freezing protocols for extracellular vesicles: a systematic review. *Stem Cell Res Ther*. 2024;15:453.
29. Zeng Y, Qiu Y, Jiang W, Shen J, Yao X, He X et al. Biological features of extracellular vesicles and challenges. *Front Cell Dev Biol*. 2022;10.
30. Wu JY, Li YJ, Hu X, Bin, Huang S, Xiang DX. Preservation of small extracellular vesicles for functional analysis and therapeutic applications: a comparative evaluation of storage conditions. *Drug Deliv*. 2021;28.
31. Xia T, Fu S, Yang R, Yang K, Lei W, Yang Y et al. Advances in the study of macrophage polarization in inflammatory immune skin diseases. *J Inflamm (United Kingdom)*. 2023;20.
32. Luo M, Zhao F, Cheng H, Su M, Wang Y. Macrophage polarization: an important role in inflammatory diseases. *Front Immunol*. 2024;15.
33. Dillingham MR, Van Poelgeest EP, Malone KE, Kemper EM, Stroes ESG, Moerland M et al. Characterization of inflammation and immune cell modulation induced by low-dose LPS administration to healthy volunteers. *J Inflamm (United Kingdom)*. 2014;11.
34. Carregosa D, Loncarevic-Vasiljkovic N, Feliciano R, Moura-Louro D, Mendes CS, dos Santos CN. Locomotor and gait changes in the LPS model of neuroinflammation are correlated with inflammatory cytokines in blood and brain. *J Inflamm*. 2024;21:39.
35. Wu CH, Chen TL, Chen TG, Ho WP, Chiu WT, Chen RM. Nitric oxide modulates pro- and anti-inflammatory cytokines in lipopolysaccharide-activated macrophages. *J Trauma*. 2003;55.
36. Zamyatina A, Heine H. Lipopolysaccharide recognition in the crossroads of TLR4 and Caspase-4/11 mediated inflammatory pathways. *Front Immunol*. 2020;11.
37. Malvicini R, Santa-Cruz D, De Lazzari G, Tolomeo AM, Sanmartin C, Muraca M et al. Macrophage bioassay standardization to assess the anti-inflammatory activity of mesenchymal stromal cell-derived small extracellular vesicles. *Cytotherapy*. 2022;24.
38. Xue R, Xie M, Wu Z, Wang S, Zhang Y, Han Z et al. Mesenchymal stem cell-derived exosomes promote recovery of the facial nerve injury through regulating macrophage M1 and M2 polarization by targeting the P38 MAPK/NF- $\kappa$ B pathway. *Aging Dis*. 2024;15.
39. Luan Z, Liu J, Li M, Wang Y, Wang Y. Exosomes derived from umbilical cord-mesenchymal stem cells inhibit the NF- $\kappa$ B/MAPK signaling pathway and reduce the inflammatory response to promote recovery from spinal cord injury. *J Orthop Surg Res*. 2024;19.
40. Jiang Y, Hong S, Zhu X, Zhang L, Tang H, Jordan KL et al. IL-10 partly mediates the ability of MSC-derived extracellular vesicles to attenuate myocardial damage in experimental metabolic renovascular hypertension. *Front Immunol*. 2022;13.
41. Eldahshan OA, Azab SS. Anti-inflammatory effect of apigenin-7-neohesperidide (rhoifolin) in carrageenin-induced rat oedema model. *J Appl Pharm Sci*. 2012;2.
42. McLean DJ, Diaz-Gil D, Farhan HN, Ladha KS, Kurth T, Eikermann M. Dose-dependent association between intermediate-acting neuromuscular-blocking agents and postoperative respiratory complications. *Anesthesiology*. 2015;122.
43. Cano NJ, Sabouraud AE, Debray M, Schermann JMG. Dose-dependent reversal of digoxin-inhibited activity of an in vitro Na<sup>+</sup>+K<sup>+</sup> ATPase model by digoxin-specific antibody. *Toxicol Lett*. 1996;85.
44. Tang Y, Zhou Y, Li HJ. Advances in mesenchymal stem cell exosomes: a review. *Stem Cell Res Therapy*. 2021;12.
45. Lotfy A, AboQuella NM, Wang H. Mesenchymal stromal/stem cell (MSC)-derived exosomes in clinical trials. *Stem Cell Res Ther*. 2023;14:66.
46. Wu JY, Wu SN, Zhang LP, Zhao XS, Li Y, Yang QY et al. Stem cell-derived exosomes: a new method for reversing skin aging. *Tissue Eng Regenerative Med*. 2022;19.
47. Bicer M. Revolutionizing dermatology: harnessing mesenchymal stem/stromal cells and exosomes in 3D platform for skin regeneration. *Arch Dermatol Res*. 2024;316:242.
48. Petiti J, Revel L, Divieto C. Standard operating procedure to optimize resazurin-based viability assays. *Biosensors*. 2024;14.
49. Goegan P, Johnson G, Vincent R. Effects of serum protein and colloid on the alamarBlue assay in cell cultures. *Toxicol Vitro*. 1995;9.
50. Azzout-Marniche D, Chalvon-Demersay T, Pimentel G, Chaumontet C, Nadkarni NA, Piedcoq J et al. Obesity-prone high-fat-fed rats reduce caloric intake and adiposity and gain more fat-free mass when allowed to self-select

- protein from carbohydrate:Fat intake. *Am J Physiol - Regul Integr Comp Physiol*. 2016;310.
51. Rising R, Lifshitz F. Energy expenditures & physical activity in rats with chronic suboptimal nutrition. *Nutr Metab*. 2006;3.
  52. Fiette L, Slaoui M, Bauchet AL. Procedures of necropsy and tissue sampling. In: *Methods in Molecular Biology*. 2017.
  53. Théry C, Witwer KW, Aikawa E, Alcaraz MJ, Anderson JD, Andriantsitohaina R et al. Minimal information for studies of extracellular vesicles 2018 (MISEV2018): a position statement of the International Society for Extracellular Vesicles and update of the MISEV2014 guidelines. *J Extracell Vesicles*. 2018;7.
  54. Yáñez-Mó M, Siljander PRM, Andreu Z, Zavec AB, Borràs FE, Buzas EI et al. Biological properties of extracellular vesicles and their physiological functions. *J Extracell Vesicles*. 2015;4.
  55. Dominici M, Le Blanc K, Mueller I, Slaper-Cortenbach I, Marini FC, Krause DS et al. Minimal criteria for defining multipotent mesenchymal stromal cells. The International Society for Cellular Therapy position statement. *Cytotherapy*. 2006;8.
  56. Bosch S, De Beaurepaire L, Allard M, Mosser M, Heichette C, Chrétien D et al. Trehalose prevents aggregation of exosomes and cryodamage. *Sci Rep*. 2016;6.
  57. Rodprasert W, Nantavisai S, Pathanachai K, Pavasant P, Osathanon T, Sawangmake C. Tailored generation of insulin producing cells from canine mesenchymal stem cells derived from bone marrow and adipose tissue. *Sci Rep*. 2021;11.
  58. Chen S, Sato Y, Tada Y, Suzuki Y, Takahashi R, Okanojo M et al. Facile bead-to-bead cell-transfer method for serial subculture and large-scale expansion of human mesenchymal stem cells in bioreactors. *Stem Cells Transl Med*. 2021;10.
  59. Wang F, Cerione RA, Antonyak MA. Isolation and characterization of extracellular vesicles produced by cell lines. *STAR Protoc*. 2021;2.
  60. Rikkert LG, Nieuwland R, Terstappen LWMM, Coumans FAW. Quality of extracellular vesicle images by transmission electron microscopy is operator and protocol dependent. *J Extracell Vesicles*. 2019;8:1555419.
  61. Padda RS, Deng FK, Brett SI, Biggs CN, Durfee PN, Brinker CJ et al. Nanoscale flow cytometry to distinguish subpopulations of prostate extracellular vesicles in patient plasma. *Prostate*. 2019;79.
  62. Villatoro AJ, Alcoholado C, Martín-Astorga MDC, Rico G, Fernández V, Becerra J. Characterization of the secretory profile and exosomes of limbal stem cells in the canine species. *PLoS ONE*. 2020;15 12 December.
  63. Silva AM, Lázaro-Ibáñez E, Gunnarsson A, Dhande A, Daaboul G, Peacock B et al. Quantification of protein cargo loading into engineered extracellular vesicles at single-vesicle and single-molecule resolution. *J Extracell Vesicles*. 2021;10.
  64. Desgeorges A, Hollerweger J, Lassacher T, Rohde E, Helmbrecht C, Gimona M. Differential fluorescence nanoparticle tracking analysis for enumeration of the extracellular vesicle content in mixed particulate solutions. *Methods*. 2020;177.
  65. Oontawee S, Phonprapai C, Itharat A, Asasutjarit R, Davies NM. Mucus-penetrating nanovesicles encapsulating a novel anti-inflammatory recipe as a transmucosal remedy: herbal extract preparation, synergistic combination, and niosomal encapsulation. *J Herb Med*. 2023;40:100670.

### Publisher's note

Springer Nature remains neutral with regard to jurisdictional claims in published maps and institutional affiliations.